CARBON 54 (2013) 86–93

Available at www.sciencedirect.com

SciVerse ScienceDirect

journal homepage: www.elsevier.com/locate/carbon

Theoretical Raman intensity of the G and 2D bands of strained graphene

Valentin N. Popov [a,*], *Philippe Lambin* [b]

[a] *Faculty of Physics, University of Sofia, BG-1164 Sofia, Bulgaria*
[b] *Research Center in Physics of Matter and Radiation, University of Namur (FUNDP), B-5000 Namur, Belgium*

ARTICLE INFO

Article history:
Received 3 July 2012
Accepted 4 November 2012
Available online 23 November 2012

ABSTRACT

The Raman G and 2D bands of uniaxially strained graphene are studied within a non-orthogonal tight-binding model for parallel scattering geometry and laser photon energy of 2.5 eV. The derived strain rate of the G band, as well as its intensity as a function of the strain direction and light polarization angle, are found in very good agreement with previous reports. The simulated 2D band shows a complex peak structure with two or three resolved subbands. The dependence of the strain rate and the Raman intensity of the latter on the strain direction and light polarization angle follows simple trigonometric expressions. Noticeable deviations from these expressions are observed for the polarization angle dependence. It is also shown quantitatively that the contribution to the 2D band of the "inner" processes is about 10 times larger than that of the "outer" processes. Our predictions for the 2D band behavior of strained graphene can be used for monitoring the strain in graphene-based applications by Raman spectroscopy.

1. Introduction

The application of mechanical forces on graphene can modify its electronic and vibrational properties, which makes this material suitable as a building block for nanoelectronic devices [1]. The monitoring of the changes of these properties is most easily done by Raman scattering of light by phonons [2]. The only first-order Raman band – the G band, is known to soften and split in graphene subjected to uniaxial tensile strain [3,4]. On the experimental side, this property can be used to determine the orientation of a sample and to calibrate its strain [5], with the uncertainty that the G band is sensitive to other perturbations such as doping [6]. The shift rate and the polarization dependence of this band have been studied in detail [3].

The most intense Raman feature in the second-order spectra is observed at about 2700 cm^{-1}. It is called the 2D band and is excited by a double-resonant Raman process [7]. The 2D band, similarly to the G band, softens and splits under uniaxial tensile strain but has a more complicated peak structure under strain, which depends on the laser photon energy and polarization in addition to the strain magnitude and direction [5,8,9].

The theoretical investigations have so far been limited mainly to the calculation of the electronic structure and the phonon dispersion of uniaxially strained graphene [5,8–10]. In one case, the calculated intensity of the 2D band has also been reported [11]. Despite the success in the understanding of the 2D band, there is still a current controversy about the dominant contribution to its Raman intensity. The behavior of the Raman 2D band of strained graphene at different strains and Raman scattering conditions has not been predicted systematically so far.

Here, the Raman intensity, shift rate and polarization dependence of the G band and 2D band of graphene, subjected to in-plane uniaxial tensile strain, are investigated

* *Corresponding author:* Fax: +359 2 96 25 276.
E-mail address: vpopov@phys.uni-sofia.bg (V.N. Popov).
0008-6223/$ - see front matter
http://dx.doi.org/10.1016/j.carbon.2012.11.006

within a non-orthogonal tight-binding (NTB) model, which has already been applied successfully to the study of the electronic and vibrational properties of carbon nanotubes and graphene. In Section 2, the computational details are presented. Section 3 is devoted to the discussion of the obtained results in comparison with available experimental and theoretical data. We show that the shift rate and the polarization dependence of the 2D band follow simple trigonometric expressions. The paper ends up with conclusions (Section 4).

2. Computational details

The calculation of the G and 2D Raman bands of strained and unstrained graphene is performed within the NTB model [12]. This model uses Hamiltonian and overlap matrix elements derived from density-functional theory applied to carbon dimers [13] and is parameter-free. Another major advantage of the NTB model in comparison with other tight-binding models is the possibility to calculate the total energy of the structure as well as the forces on the atoms. This property allows one to relax the atomic structure of unstrained and strained materials. The relaxation of the structure is mandatory for phonon dispersion calculation. The total energy for structure relaxation is obtained by summation of the band energies over a 40×40 uniform mesh of wavevectors in the Brillouin zone of graphene.

Within a few electron volts away from the Fermi energy, the conduction and valence bands of graphene are approximately conic-like (Dirac cones) with a common vertex at the two nonequivalent special points K and K′ of the Brillouin zone. This specific electronic structure predetermines the importance of the Dirac cones for optical processes in graphene. In particular, the Raman 2D band arises from double-resonant scattering of electrons and holes from phonons between states located on the Dirac cones at the K and K′ points.

The NTB model is extended to calculation of the phonon dispersion of graphene by using a perturbative approach [14]. The convergence of the phonon frequencies within $1\ cm^{-1}$ is achieved by summation of the perturbative terms of the dynamical matrix over the aforementioned 40×40 mesh of wavevectors in the Brillouin zone. The derived phonon frequencies overestimate the experimental values of the in-plane optical phonon branches, which is a common feature of most tight-binding models. For these branches, reasonable agreement of our phonon frequencies with the experimental data is achieved by multiplication by a factor of 0.9 (for detailed comparison of the NTB phonon dispersion with available experimental and theoretical data, see Refs. [14,15]). This scaling is implied everywhere below. The doubly degenerate in-plane optical phonon at the Γ point – herein called the G mode – is responsible for the Raman G band, whereas phonon modes arising from the in-plane transverse optical (iTO) branch close to the K and K′ points contribute to the 2D band (Fig. 1). The G band is calculated by using third-order quantum-mechanical perturbation terms with electron/hole-photon matrix element and electron/hole lifetime, derived within the NTB model [16]. The summation over the electron wavevector for the lifetime is performed on a 800×800 uniform mesh of wavevectors in the entire Brillouin zone.

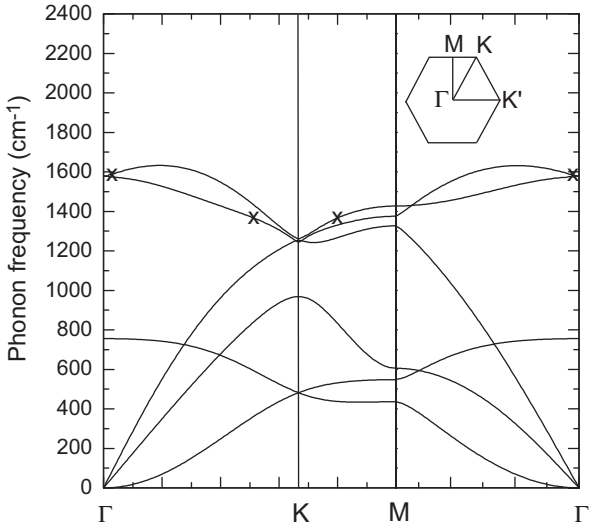

Fig. 1 – The NTB phonon dispersion of graphene along the ΓK, ΓM, and KM directions in the Brillouin zone of graphene. The G band originates from the doubly degenerate in-plane optical phonon at the Γ point (see cross mark). The 2D band arises from double-resonant scattering of electrons and holes by phonons belonging to the iTO branch close to the K and K′ points of the Brillouin zones. The term "inner" ("outer") is used for scattering processes mediated by phonons with wavevectors around the ΓK (KM) direction close to the K point (see cross marks). Inset: the hexagonal first Brillouin zone of graphene.

The 2D band is known to arise from double-resonant scattering processes with participation of two phonons [7]. Each process consists of several virtual ones: absorption of an incident photon with creation of an electron–hole pair, double scattering of the created electron/hole by phonons, and recombination of the electron–hole pair with emission of a photon. Altogether, there are eight such processes [17,18] and all of them are taken into account in the calculation of the Raman intensity of the 2D band below. The phonons, contributing to the 2D band, belong to the iTO branch close to the ΓK and KM directions (see Fig. 1). The scattering processes of electrons and holes by these phonons are usually termed "inner" and "outer", respectively. The role of these processes in the double-resonant Raman spectra has been discussed extensively in the literature [11,18,19]. Recently, we have calculated the contribution of the two types of processes to the integrated intensity of this band and have shown that the "inner" processes have much larger contribution than the "outer" ones for laser photon energies E_L between 1.0 eV and 3.5 eV [19]. In this work, the "outer" processes are considered explicitly, despite their relatively small contribution.

The calculation of the Raman 2D band intensity is carried out using fourth-order quantum-mechanical perturbation terms [20]. The latter include electron/hole-photon and electron/hole-phonon matrix elements, and electron/hole lifetime, obtained within the NTB model. The computational procedure includes summation over the electronic wavevector for a fixed phonon wavevector and a subsequent summation over the phonon wavevector and over the transverse

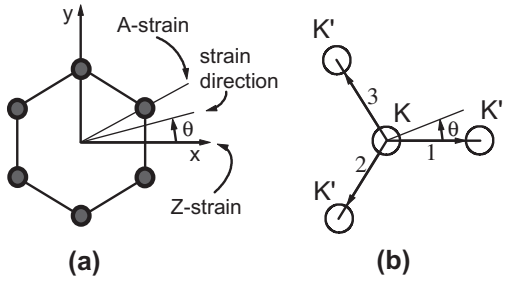

Fig. 2 – (a) The atomic structure of graphene. The circles and the connecting lines between them denote carbon atoms and carbon–carbon bonds, respectively. The direction of the uniaxial strain is defined by the angle θ relative to a zigzag of carbon bonds. The limiting cases of Z-strain ($\theta = 0°$) and A-strain ($\theta = 30°$) are also shown. (b) A part of the Brillouin zone of graphene with the K point and the closest three K′ points. The three different scattering paths for electrons and holes between the Dirac cones at the K and K′ points (empty circles), which contribute to the 2D band intensity, are denoted by the numbers 1, 2, and 3.

phonon branch. The two summations are performed over the entire Brillouin zone and convergence is achieved by resorting to a 800×800 uniform mesh of wavevectors [19].

We focus on in-plane uniaxially strained graphene. The strain direction is defined by its angle θ with respect to a zigzag line of carbon atoms (Fig. 2a). At $\theta = 0$, the two-dimensional in-plane strain tensor ε has two nonzero components: $\varepsilon_{11} = \varepsilon$ and $\varepsilon_{22} = -\nu\varepsilon$, where ν is Poisson's ratio. For $\theta \neq 0$, the strain tensor can be obtained by an orthogonal transformation [10]. The distinct strain directions can be characterized by values of θ between 0° (zigzag strain or Z-strain) and 30° (strain along an armchair line of carbon bonds or A-strain). We consider strain with magnitude $\varepsilon = 1\%$ and direction angle $\theta = 0°$, 10°, 20° and 30°.

The G and 2D band intensity is calculated for a single value of E_L of 2.5 eV, which is close to the laser photon energies frequently used in Raman experiments. We focus our investigation on Stokes processes in the parallel scattering geometry. The common value of the polarizer angle φ_L and the analyzer angle φ_S will be denoted by φ. The angle φ is defined relative to the strain direction, unless stated otherwise.

3. Results and discussion

3.1. *The G band*

In strained graphene, the G band splits into two subbands [3]. The higher (lower)-frequency one is denoted by G^+ (G^-), in analogy to those in carbon nanotubes. The atomic displacements for the G^+ (G^-) subband are perpendicular (parallel) to the strain direction. The shift rates $\partial\omega_{G^\pm}/\partial\varepsilon$ are independent of the strain direction because of the high in-plane symmetry of graphene. Here, we obtain the following shift rates: $\partial\omega_{G^+}/\partial\varepsilon = -20.6\ \mathrm{cm^{-1}/\%}$ and $\partial\omega_{G^-}/\partial\varepsilon = -39.4\ \mathrm{cm^{-1}/\%}$. Recent precise Raman measurements have allowed to derive the following pairs of values for the shift rates (−18.6, −36.4) $\mathrm{cm^{-1}/\%}$ (Ref. [3]), in excellent agreement with the ab-initio values (−17, −34) $\mathrm{cm^{-1}/\%}$ (Ref. [3]), (−14.5, −34) $\mathrm{cm^{-1}/\%}$ (Ref. [4]), (−5.6, −12.5) $\mathrm{cm^{-1}/\%}$ (Ref. [5]), (−9.6, −31.4) $\mathrm{cm^{-1}/\%}$ (Ref. [8]), (−13.7, −33.2) $\mathrm{cm^{-1}/\%}$ (averaged values for two samples with almost Z and A-strain, Ref. [9]). The overestimation of our rates can be reduced to match most of the experimental and theoretical ones by multiplication by a factor of 0.9: $\partial\omega_{G^+}/\partial\varepsilon = -18.5\ \mathrm{cm^{-1}/\%}$ and $\partial\omega_{G^-}/\partial\varepsilon = -35.5\ \mathrm{cm^{-1}/\%}$. To clarify the origin of this overestimation, we note that the shift rate is determined by the derivative of the dynamical matrix with respect to the strain. In the perturbative approach, the dynamical matrix is expressed through the electron–phonon matrix elements. As in similar parameter-free tight-binding models, the band energy includes only a part of the electron–electron interaction energy, while the remaining part is described by pair potentials [13]. Thus, a part of the electronic response to the atomic displacements and strain are not accounted for properly and the phonon frequencies and shift rates are stiffer than the real ones. Furthermore, it can be expected that similar overestimation may be present for the shift rate of the 2D band as well.

The secular equation for the G mode under strain yields the $G^\pm$ mode shift rate as [3]

$$\partial\omega_{G^\pm}/\partial\varepsilon = -\omega_G\gamma_G(1-\nu) \pm \omega_G\beta_G(1+\nu)/2 \quad (1)$$

Here, ω_G is the G mode frequency at zero strain, γ_G is the Grüneisen parameter, and β_G is the shear deformation potential of the G mode. From Eq. (1) one gets

$$\gamma_G = -(\partial\omega_{G^+}/\partial\varepsilon + \partial\omega_{G^-}/\partial\varepsilon)/[2\omega_G(1-\nu)] \quad (2)$$

$$\beta_G = (\partial\omega_{G^+}/\partial\varepsilon - \partial\omega_{G^-}/\partial\varepsilon)/[\omega_G(1+\nu)] \quad (3)$$

Inserting our calculated values $\omega_G = 1590\ \mathrm{cm^{-1}}$ and $\nu = 0.281$ in Eqs. (2) and (3), we obtain $\gamma_G = 2.64$ and $\beta_G = 0.93$ (or $\gamma_G = 2.36$ and $\beta_G = 0.84$ after scaling of the shift rates by 0.9). Recent Raman measurements yield the values $\gamma_G = 1.99$ and $\beta_G = 0.99$ (Ref. [3]), and $\gamma_G = 2.2$ and $\beta_G = 0.93$ (Ref. [9]), which agree with the ab-initio ones of $\gamma_G = 1.87$ and $\beta_G = 0.92$ [3]. As expected for most tight-binding models, the NTB values of the Grüneisen parameter and the shear deformation potential deviate from the published data.

The Raman intensity of the G band of unstrained graphene is independent of the polarization angles φ_L and φ_S because of the high in-plane symmetry of graphene [21]. Indeed, the angular dependence of the G band can be determined from the formula for the intensity: $I \propto \sum_{i=1}^{2}|\mathbf{e}_S \cdot (R \cdot \mathbf{e}_i) \cdot \mathbf{e}_L|^2$, where e_L and e_S are the polarization vectors of the incident and scattered light, respectively, e_i is the phonon polarization vector of the ith component of the G mode (i = 1, 2), and the third rank tensor R is the Raman scattering amplitude. In the case of the two-dimensional hexagonal space group of graphene [22], the nonzero components of R are $R_{xxy} = -R_{yyy} = R_{xyx} = R_{yxx}$ (see, e.g., Ref. [23]). Choosing the light polarization vectors in the form $e_L = (\cos\varphi_L, \sin\varphi_L)$ and $e_S = (\cos\varphi_S, \sin\varphi_S)$, and assuming that the polarization of the components of the G mode is given by $e_1 = (\cos\delta, \sin\delta)$ and $e_2 = (-\sin\delta, \cos\delta)$, where δ is an arbitrary angle, we can rewrite the intensity as

$$I_G \propto \cos^2(\varphi_S + \varphi_L + \delta) + \sin^2(\varphi_S + \varphi_L + \delta) = 1 \quad (4)$$

Therefore, the Raman intensity of unstrained graphene is independent of the polarization angles.

For strained graphene, we can still use the results for unstrained graphene obtained above. It is convenient to define the angles δ, φ_L, and φ_S with respect to the strain direction: $\delta \to \delta + \theta$, $\varphi_L \to \varphi_L + \theta$, and $\varphi_S \to \varphi_S + \theta$. In strained graphene, the G^- and G^+ components of the G mode become strictly longitudinal (l) and transverse (t) with respect to the strain direction, i.e., $\delta = 0$. Then, the polarization dependence of the intensity of the $G^\pm$ bands can be written as (see also Ref. [3])

$$I_{G^-} \propto \sin^2(\varphi_L + \varphi_S + 3\theta) \quad (5)$$

$$I_{G^+} \propto \cos^2(\varphi_L + \varphi_S + 3\theta) \quad (6)$$

Fig. 3 shows that, for parallel scattering geometry, Eqs. (5) and (6) can be fitted perfectly to the calculated intensity of the $G^\pm$ bands. We note that the integrated intensity of the two bands (not given) also follows the two equations above. The very good agreement of our results for the G band with available experimental and theoretical data gives us confidence that the NTB model can be used for quantitative description of the second-order Raman spectra of strained graphene as well. In Section 3.2, the application of this model to the 2D band is presented.

3.2. *The 2D band*

For unstrained graphene we obtain $\omega_{2D} = 2744.7\ cm^{-1}$. From Raman measurements data [21,15] one derives $\omega_{2D} \approx 2694\ cm^{-1}$ at $E_L = 2.5$ eV. Therefore, at this value of E_L, there is an overestimation of the 2D band frequency by about $51\ cm^{-1}$. The ab-initio calculations also predict higher frequencies than the observed ones, unless GW effects are included [18].

In view of the current controversy regarding the relative contributions of the "inner" and "outer" processes to the 2D band, it is important to determine quantitatively their ratio within the NTB model. According to the accepted definition, the "inner" ("outer") processes involve phonons with wavevectors near the ΓK (KM) direction close to the K point and belonging to the iTO branch. The other branches close to the latter at the K point have negligible electron–phonon matrix element and do not contribute to the Raman spectra [18,19]. Numbering the phonon branches in order of increasing frequencies, the iTO branch is the 5th near the ΓK direction and the 6th near the KM directions (see cross marks in Fig. 1). Therefore, the contribution of the "inner" processes is obtained by considering only the 5th branch, while the contribution of the "outer" processes is obtained by considering only the 6th branch near the K point. The calculations show that the contribution of the "outer" processes is redshifted with respect to that from "inner" processes (Fig. 4, top). The predicted shift of $8.3\ cm^{-1}$ is in agreement with the previously calculated one of $9.2\ cm^{-1}$ [10] and with the shift of about $10\ cm^{-1}$ experimentally measured at $E_L = 1.58$ eV [8].

In strained graphene, the 2D band should split into 12 subbands arising from scattering paths 1, 2, and 3, and "inner" and "outer" processes for electrons and holes for each path. However, because of the approximate electron–hole symmetry, the number of resolved subbands is reduced to six [8,10]. As an example, Fig. 4 (bottom panels) shows typical 2D bands calculated at $\theta = 20°$ and polarization angles $\varphi = 0°$ and 90°. For each of the bands, it is impossible to identify more than two (or three) subbands. In all cases, the contribution of "inner" processes to the 2D band is about 10 times lar-

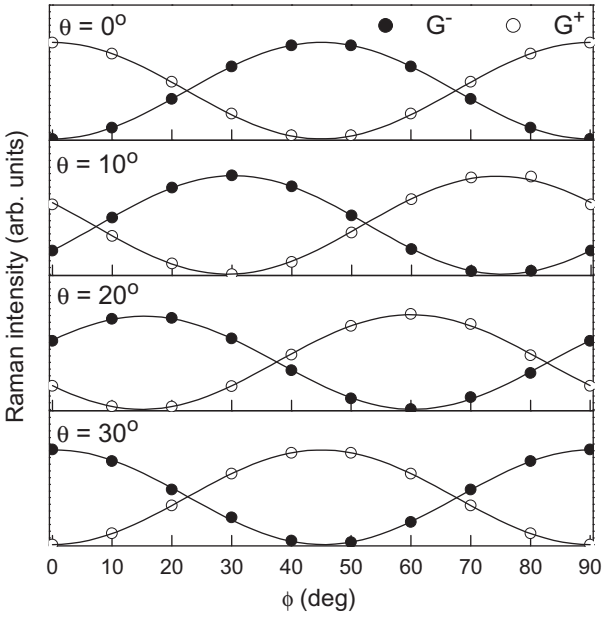

Fig. 3 – The calculated Raman intensity of the G^- and G^+ bands in strained graphene for parallel scattering geometry as a function of the light polarization angle φ at strain angles $\theta = 0°$, 10°, 20° and 30°. The solid lines are best fit of Eqs. (5) and (6) to these data.

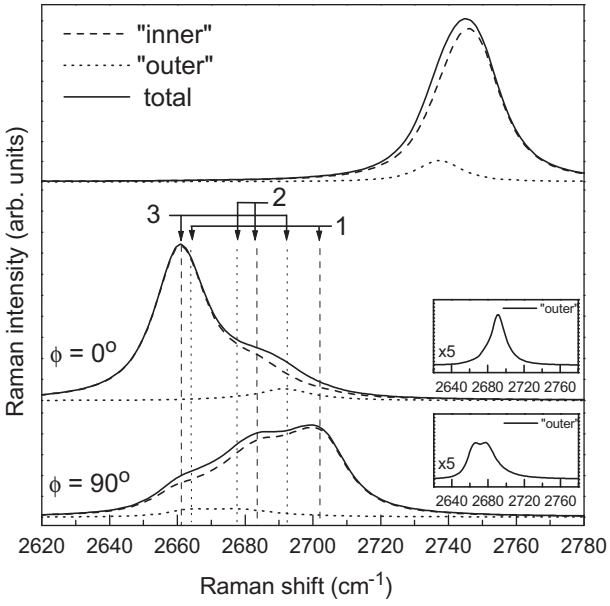

Fig. 4 – The 2D band at $\theta = 20°$ and polarizations $\varphi = 0°$ and $\varphi = 90°$ (bottom panels) in comparison with the 2D band for unstrained graphene, where the ratio of the integrated intensities for the "inner" and "outer" processes is ≈10 (top panel). The six resolved subbands due to "inner" and "outer" processes 1, 2 and 3 are marked by vertical lines. The scale is the same for all graphs. The insets show the scaled contributions to the spectra from the "outer" processes.

ger than that of "outer" processes. The overall effect of the "outer" processes is to deform slightly the shape of the subbands. This behavior persists for all the studied strain directions and polarization angles, and can be accepted as a general feature of the 2D band. As in Ref. [18], we find that the obtained larger contribution of the "inner" processes is due to the explicit account of the matrix elements in the intensity calculations [14]. The conclusion for the dominant contribution of the "inner" processes is supported by the combined analysis of experimental 2D Raman bands and theoretical results on the corresponding shift rates [9]. This point is not shared by all researchers in the area, however, as can be seen from the on-going discussion in the literature. Recently, it has been concluded from precise Raman measurements that the "inner" and "outer" contributions to the Raman signal at $E_L = 1.58$ eV are comparable [8]. In another study [11], it is stated that the "inner" and "outer" contributions to the 2D band are polarization-dependent but this point has not been discussed quantitatively. The reasons for the existing contradictory conclusions can also be sought in the lack of a strict computational procedure allowing quantitative distinction between the contributions of the "inner" and "outer" processes, as the one proposed above and in Ref. [19].

Fig. 5 shows the evolution of the calculated 2D band for four different values of θ. We use only two (or three) Lorentzian functions for the two (or three) distinct 2D subbands, for which we adopt the notation $2D_1$, $2D_2$, and $2D_3$, in order of decreasing frequencies. They originate from "inner" and "outer" scattering processes of electrons and holes by phonons in

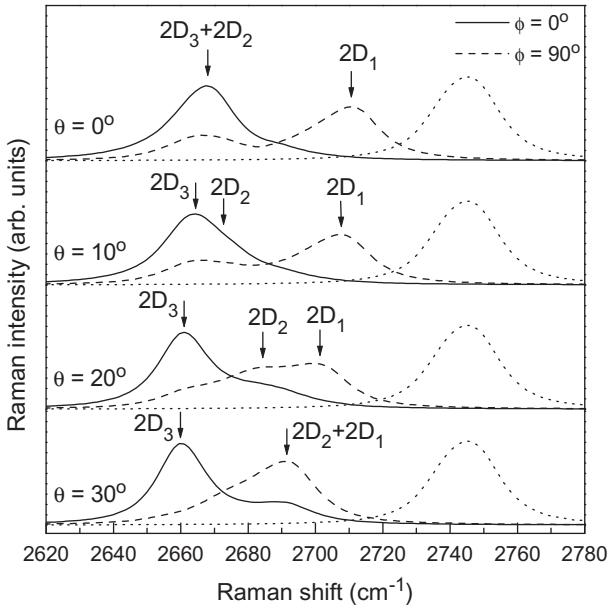

Fig. 5 – The calculated Raman spectra of uniaxially strained graphene in the 2D band range at $\theta = 0°$, 10° 20° and 30°. The continuous (dashed) line is the 2D band for parallel (perpendicular) light polarization relative to the strain direction. The dotted line is the 2D band for unstrained graphene. The arrows mark the Raman shift of the two (three) components of the 2D band. The scale is the same for all graphs.

the three paths labeled by 1, 2, and 3 in Fig. 2b. Thus, at $\theta = 0°$, there are two distinct 2D subbands: paths 2 and 3 give rise to the lower-frequency one and path 1 is responsible for the higher-frequency subband. At $\theta = 10°$ and $\theta = 20°$, an intermediate subband appears due to path 2. Finally, at $\theta = 30°$, there remain again two subbands: a lower-frequency one coming from path 3 and a higher-frequency one coming from paths 1 and 2. Thus, with the increase of θ from Z-strain to A-strain, the subband due to path 2 shifts from the lower-frequency band to the higher-frequency one. With the increase of the polarization angle φ from zero to 90°, the intensity of the lowest-frequency subband decreases and that of the highest-frequency one increases. The splitting between these two subbands decreases with increasing θ. The width at half maximum of each of the three subbands varies between 16 and 29 cm^{-1}.

The experimental Raman 2D band exhibits either one-peak [5] or two-peak [8,9] structure, depending on the laser photon energy, while a three-peak structure has never been observed. The simulated spectra have common features with the observed ones, namely, the lower-frequency subband is more intense than the higher-frequency one at $\varphi = 0°$ and vice versa at $\varphi = 90°$. For Z-strain, the splitting is larger than for A-strain [8,9]. Moreover, our results correspond qualitatively to the experimental observation at $E_L = 2.33$ eV that for Z-strain the low frequency subband retains about half of its maximum intensity upon increasing of φ from 0° to 90°, whereas the high frequency one is almost absent at $\varphi = 0°$, and vice versa for A-strain [5]. As far as we know, the literature reports but one simulation of the Raman intensity of the 2D band, using fourth-order quantum perturbation terms within the density-functional theory approach [11]. The results, obtained in that paper, were found to overestimate consistently the intensity of the sidebands, which was attributed to the functional used in this approach. In particular, the ratio of the integrated intensity of the two subbands for Z-strain at $\varphi = 0°$ has been predicted close to one, which disagrees with the experimental data and with our results.

The Raman shift and the integrated intensity of the 2D subbands are derived by fitting the spectra of Fig. 5 with two or three Lorentzian functions. Fig. 6 shows the obtained Raman shifts of the $2D_1$, $2D_2$, and $2D_3$ subbands as a function of the angle θ. These data can be fitted nicely with the expressions

$$\omega_{2D_1} = A + B\sin^4(\theta + \pi/2) \quad (7)$$

$$\omega_{2D_2} = A + B\sin^4(\theta + \pi/6) \quad (8)$$

$$\omega_{2D_3} = A + B\sin^4(\theta - \pi/6) \quad (9)$$

where $A = 2661.4$ cm^{-1} and $B = 51.0$ cm^{-1}.

Assuming linear dependence of $\omega_{2D_{1,2,3}}$ on ε, the shift rates $\partial\omega_{2D_1}/\partial\varepsilon$, $\partial\omega_{2D_2}/\partial\varepsilon$, and $\partial\omega_{2D_3}/\partial\varepsilon$ at $\theta = 0°$, 10°, 20° and 30° follow readily from Eqs. (7)–(9). In particular, for Z and A-strain, the pairs of shift rates are (−32.3, −80.1) and (−54.6, −83.3) cm^{-1}/%, respectively. By comparison, a single shift rate of −64 cm^{-1}/% has been derived recently for the 2D band of a large set of samples measured at $E_L = 2.41$ eV [3]. For Z and A-strain samples measured at $E_L = 2.33$ eV, the following shift rates have been obtained: (−16.3, −29.7) and (−21.7, −30.5)

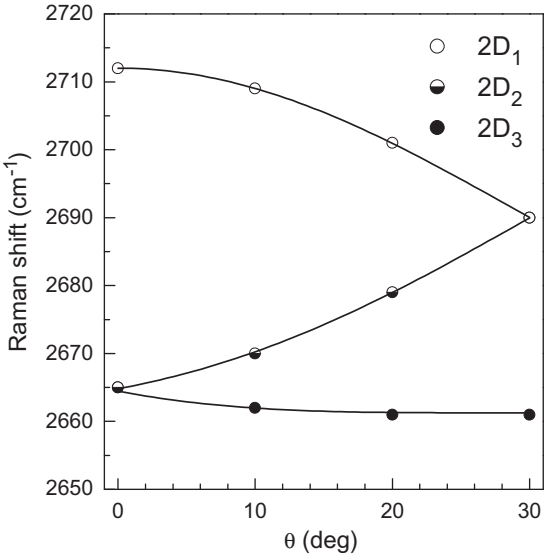

Fig. 6 – The calculated Raman shifts of the $2D_1$, $2D_2$, and $2D_3$ subbands at $\theta = 0°$, 10°, 20° and 30° (circles). The solid lines are fits of Eqs. (7)–(9) to the calculated data.

cm^{-1}/%, respectively [5]. For a sample with $\theta = 18.4°$ measured at $E_L = 1.58$ eV, the shift rates (−23.6, −46.8) cm^{-1}/% have been determined [8]. For Z and A-strain samples measured at $E_L = 2.41$ eV, the established pairs of shift rates are: (−26.0, −67.8) and (−44.1, −63.1) cm^{-1}/%, respectively, and the calculated ones are (−24, −66) and (−43, −70) cm^{-1}/%, respectively [9]. Among all the reported data, the shift rates of Ref. [5] are the smallest (in absolute value), which could be due to the small G^- and G^+ band shift rates of −12.5 and −5.6 cm^{-1}/%, respectively, used to calibrate the strain. It is clear that our values for the shift rates are larger (in absolute value) than all the reported ones. Accepting the same scaling factor of 0.9 as for the shift rate of the $G^\pm$ subbands, our pairs of shift rates for Z and A-strain become (−29.1, −72.1) and (−49.1, −75.0) cm^{-1}/%, respectively. These values are still larger by a few percent than the largest reported ab-initio ones of Ref. [9]. The correct scaling factors for the shift rates of the G and 2D bands can be deduced in future based on more precise experimental data and theoretical results.

From our values for the shift rates, it follows that the difference of the Raman shifts of the two subbands for Z-strain is $5/3 \approx 1.67$ times larger than for A-strain. This result agrees both with the ratio of 2.2 measured at $E_L = 2.41$ eV and with the predicted value of 1.6 [9]. The measured Raman shift of the lower-frequency subband for Z-strain (in absolute value) is larger than that for A-strain, whereas Ref. [9] and the present work predict the opposite.

Next, we discuss the polarization dependence of the 2D subbands. It has been shown by first-order time-dependent perturbation theory [24] that the electron-photon matrix element is proportional to the vector product of the electron wavevector k with respect to the K or K′ point and the light polarization vector e: $k \times e_{L,S}$. Thus, the polarization dependence of the Raman intensity of the 2D band is determined by the product of the squared sines between k and $e_{L,S}$. In the double-resonant processes, contributing to the 2D band, an electron (a hole) is scattered between states on the Dirac cones at the K and K′ points. Therefore, the direction of k is fixed by the vectors denoted by 1, 2, and 3 in Fig. 2b and the Raman intensity has the following polarization dependence

$$I_{2D} \propto \sin^2\varphi_L \sin^2\varphi_s + \sin^2(\varphi_L + 2\pi/3)\sin^2(\varphi_s + 2\pi/3) + \sin^2(\varphi_L - 2\pi/3)\sin^2(\varphi_s - 2\pi/3) \quad (10)$$

This expression can easily be transformed to the simpler one (see, also Refs. [19,21])

$$I_{2D} \propto 2\cos^2(\varphi_L - \varphi_S) + 1 \quad (11)$$

It follows from Eq. (11) that the ratio of the intensity for cross and parallel polarization equals to 1/3.

In the case of strained graphene, we can still use Eq. (10) for the intensity. Assuming that the effect of the strain on the electronic structure can be described as a rigid displacement of the Dirac cones [5,9], we can write the intensity of the 2D subbands as (compare to Ref. [5])

$$I_{2D_1} \propto \sin^2(\varphi_L + \theta)\sin^2(\varphi_S + \theta) \quad (12)$$

$$I_{2D_2} \propto \sin^2(\varphi_L + \theta + 2\pi/3)\sin^2(\varphi_S + \theta + 2\pi/3) \quad (13)$$

$$I_{2D_3} \propto \sin^2(\varphi_L + \theta - 2\pi/3)\sin^2(\varphi_S + \theta - 2\pi/3) \quad (14)$$

In order to verify the obtained expressions for the Raman intensity of the 2D subbands, given by Eqs. (12)–(14), we performed extensive calculations (Fig. 7). The Raman spectra obtained for Z and A-strain visually correspond to the experimental ones of Ref. [9]. The integrated intensity derived from Fig. 7 is summarized in Fig. 8. The fitting of Eqs. (12)–(14) to our data was not very successful with major discrepancy taking place for intermediate polarization angles. The reason for this disagreement can be sought in the approximate

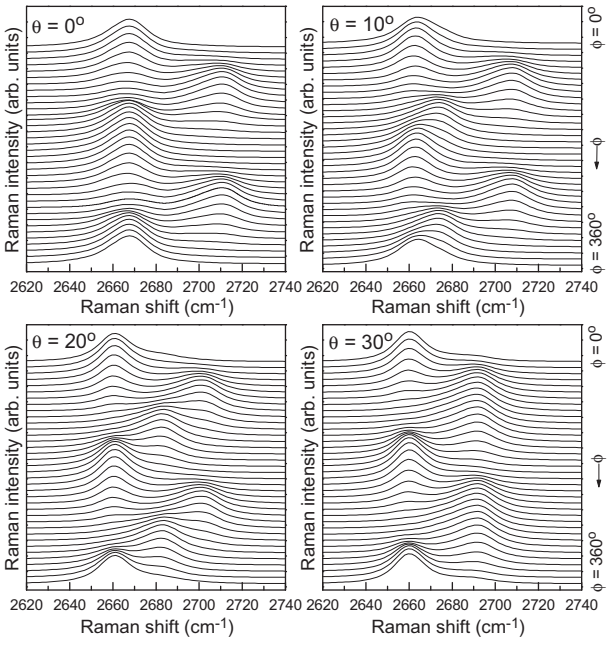

Fig. 7 – The calculated Raman spectra in the 2D band region at $\theta = 0°$, 10°, 20° and 30° for polarization angle φ varying from 0° to 180° by steps of 10°. The scale is the same for all graphs.

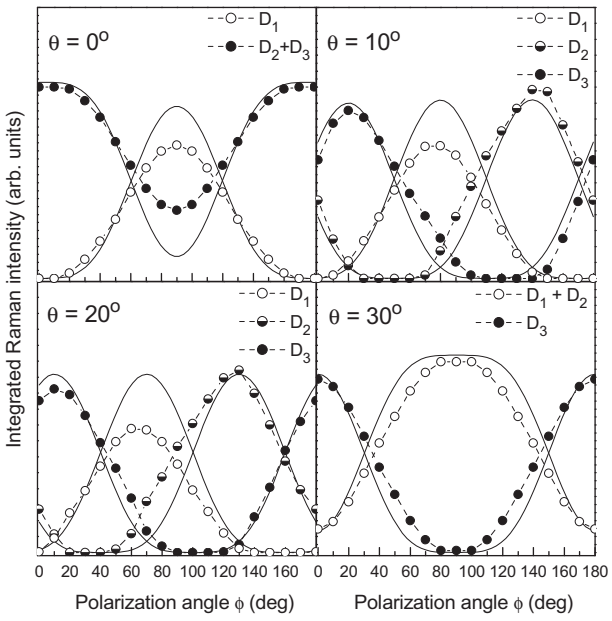

Fig. 8 – The polarization dependence of the integrated Raman intensity derived from the calculated Raman spectra plotted in Fig. 7 (circles). The dashed lines are guides to the eye. The solid lines are fits of Eqs. (12)–(14) to the calculated data. The scale is the same for all graphs.

nature of the fitting expressions. Indeed, the latter have been derived assuming rigid displacements of the Dirac cones under strain, which ignores the possible modification of the electronic band structure and phonon dispersion, as well as the electron–phonon matrix elements in strained graphene. The latter effects should be incorporated in the fitting expressions at the expense of more theoretical efforts. Our results for the shift rates of the 2D subbands agree very well with the available experimental data and we believe that this should be true for the simulated 2D band as well.

Finally, we note that the shift rate and the Raman intensity of the 2D subbands depend also on the strain magnitude ε and on the laser photon energy E_L. The results of the investigations on this dependence will be reported elsewhere.

4. Conclusions

We have presented a systematic theoretical investigation of the Raman G and 2D bands of uniaxially strained graphene for fixed strain magnitude $\varepsilon = 1\%$, parallel scattering geometry and photon laser energy $E_L = 2.5$ eV. The dependence of the shift rate of the 2D band on the strain direction is found to follow simple trigonometric expressions, while the strain direction and polarization dependence of the 2D band intensity shows deviations from the simple expressions proposed previously. In all studied cases, the contribution of the "inner" processes to the Raman spectra is about 10 times larger than that of the "outer" processes, which is corroborated by the agreement of our results with the available experimental data. Finally, the realistic description of the G and 2D bands shift rate and intensity produced by the NTB model shows that it is a reliable tool for Raman spectra simulations.

Acknowledgment

V.N.P. was supported by Grant No. 71/05.04.2012 of University of Sofia, Sofia, Bulgaria.

REFERENCES

[1] Novoselov KS, Geim AK, Morozov SV, Jiang D, Zhang Z, Dubonos SV, et al. Electric field effect in atomically thin carbon films. Science 2004;306(5696):666–9.
[2] Ferrari AC, Meyer JC, Scardaci V, Casiraghi C, Lazzeri M, Mauri F, et al. Raman spectrum of graphene and graphene layers. Phys Rev Lett 2006;97(11). 187401-1–4.
[3] Mohiuddin TMG, Lombardo A, Nair RR, Bonetti A, Savini G, Jalil R, et al. Uniaxial strain in graphene by Raman spectroscopy: G peak splitting, Grüneisen parameters, and sample orientation. Phys Rev B 2009;79(8). 205433-1–8.
[4] Mohr M, Papagelis K, Maultzsch J, Thomsen C. Two-dimensional electronic and vibrational band structure of uniaxially strained graphene from ab-initio calculations. Phys Rev B 2009;80(20). 205410-1–4.
[5] Huang M, Yan H, Heinz TF, Hone J. Probing strain-induced electronic structure change in graphene by Raman spectroscopy. Nano Lett 2010;10:4074–9.
[6] Lazzeri M, Mauri F. Nonadiabatic kohn anomaly in a doped graphene monolayer. Phys Rev Lett 2006;97(26). 266407-1–4.
[7] Reich S, Thomsen C. Raman spectroscopy of graphite. Phil Trans R Soc Lond A 2004;362:2271–88.
[8] Frank O, Mohr M, Maultzsch J, Thomsen C, Riaz I, Jalil R, et al. Raman 2D-band splitting in graphene: Theory and experiment. ACS Nano 2011;5(3):2231–9.
[9] Yoon D, Son YW, Cheong H. Strain-dependent splitting of the double-resonance Raman scattering band in graphene. Phys Rev Lett 2011;106(15). 155502-1–4.
[10] Mohr M, Maultzsch J, Thomsen C. Splitting of the Raman 2D band of graphene subjected to strain. Phys Rev B 2010;82(20). 201409(R)-1–4.
[11] Narula R, Bonini N, Marzari N, Reich S. Dominant phonon wave vectors and strain-induced splitting of the 2D Raman Mode of graphene. Phys Rev B 2012;85(11). 115451-1–5.
[12] Popov VN, Henrard L. Comparative study of the optical properties of single-walled carbon nanotubes within orthogonal and nonorthogonal tight-binding models. Phys Rev B 2004;70(11). 115407-1–12.
[13] Porezag D, Frauenheim Th, Köhler Th. Construction of tight-binding-like potentials on the basis of density-functional theory: Application to carbon. Phys Rev B 1995;51(19):12947–57.
[14] Popov VN, Lambin Ph. Radius and chirality dependence of the radial breathing mode and the G-band phonon modes of single-walled carbon nanotubes. Phys Rev B 2006;73(8). 085407-1–9.
[15] Mafra DL, Samsonidze G, Malard LM, Elias DC, Brant JC, Plentz F, et al. Determination of LA and TO phonon dispersion relations of graphene near the Dirac point by double resonance Raman scattering. Phys Rev B 2007;76(23). 233407-1–4.
[16] Popov VN, Lambin Ph. Dynamic and charge doping effects on the phonon dispersion of graphene. Phys Rev B 2010;82(4). 045406-1–9.
[17] Kürti J, Zólyomi V, Grüneis A, Kuzmany H. Double resonant Raman phenomena enhanced by van Hove singularities in single-wall carbon nanotubes. Phys Rev B 2002;65(16). 165433-1-9.

[18] Venezuela P, Lazzeri M, Mauri F. Theory of double-resonant Raman spectra in graphene: Intensity and line shape of defect-induced and two-phonon bands. Phys Rev B 2011;84(3). 035433-1–25.
[19] V.N. Popov and Ph. Lambin, Theoretical polarization dependence of the two-phonon double-resonant Raman spectra of graphene. Eur Phys J B, 2012, accepted for publication, http://dx.doi.org/10.1140/epjb/e2012-30684-x, arXiv:1206.3827v2 [cond-mat.mes-hall].
[20] Martin RM, Falicov L. In: Cardona M, editor. Light scattering in solids. Topics of applied physics, vol. 8. Berlin: Springer; 1975. p. 80–148.
[21] Yoon D, Moon H, Son YW, Samsonidze G, Park BH, Kim JB. Strong polarization dependence of double-resonant Raman intensities in graphene. Nano Lett 2008;8(12): 4270–4.
[22] Charlier JC, Eklund PC, Zhu J, Ferrari AC. Electron and phonon properties of graphene: their relationship with carbon nanotubes. In: Jorio A, Dresselhaus G, Dresselhaus MS, editors. Topics of applied physics, vol 111. Berlin: Springer; 2008. p. 673–709.
[23] Nye JF. Physical properties of crystals, their representation by tensors and matrices. Oxford: Clarendon; 1957.
[24] Grüneis A, Saito R, Samsonidze GG, Kimura T, Pimenta MA, Jorio A, et al. Inhomogeneous optical absorption around the K point in graphite and carbon nanotubes. Phys Rev B 2003;67(16). 165402-1–7.